Hindawi
Shock and Vibration
Volume 2018, Article ID 3295787, 17 pages
https://doi.org/10.1155/2018/3295787

Research Article

Dynamic Response of Pipe Conveying Fluid with Lateral Moving Supports

Baohui Li, Zhengzhong Wang, and Lina Jing

College of Water Resources and Architectural Engineering, Northwest A&F University, Yangling 712100, China

Correspondence should be addressed to Baohui Li; libaohui@nwafu.edu.cn

Received 20 June 2018; Revised 6 September 2018; Accepted 12 September 2018; Published 4 November 2018

Academic Editor: Evgeny Petrov

The Galerkin method is proposed to reveal the dynamic response of pipe conveying fluid (PCF), with lateral moving supports on both ends of the pipe. Firstly, the dynamic equation is derived by the Newtonian method after calculating the acceleration of the fluid element via the dynamics approach. Secondly, the discrete form of the dynamic equation is formulated by the Galerkin method. Thirdly, the numerical analysis of the system is carried out through the fourth-order Runge–Kutta method, and the effectiveness of the proposed method is validated by comparison with the analytical results obtained by the mode superposition method. In the example analysis, the responses of the lateral deflection and bending moment are investigated for the pinned-pinned, clamped-pinned, and clamped-clamped PCF. The effects of fluid velocity and the moving frequencies of supports are discussed. Especially, the deflection responses are analyzed under extreme condition; i.e., the moving frequency of a support is identical to the natural frequency of PCF.

1. Introduction

Transportation pipes are widely used in various industry fields, such as oil exploitation, aviation fuel piping, and nuclear plant cooling systems. The flow-induced vibration, however, seriously threatens the safe operation of the systems. Each year, the vibration-induced leakage and failure cause huge losses in the economy worldwide. Due to this reason, studies on pipe dynamics have become popular in recent years, and a new dynamical model gradually formed [1–4].

Usually, the dynamic equation of PCF can be established via the Newtonian method or generalized Hamilton's principle for an open system [5, 6]. Several dynamic models have been developed during researching PCF. To date, the researchers have already reached a consensus on the classic dynamic model of pipe, such as the linear free vibration model for PCF, which can be described by the following equation [2]:

$$EI\frac{\partial^4 w}{\partial x^4} + m_f V^2 \frac{\partial^2 w}{\partial x^2} + 2m_f V \frac{\partial^2 w}{\partial x \partial t} + \left(m_f + m_p\right)\frac{\partial^2 w}{\partial t^2} = 0. \tag{1}$$

At present, three aspects, i.e., the numerical solution techniques, pipe dynamic characters, and the extended dynamic model for more specific problems, attract much attention. For instance, Sreejith et al. [7] proposed the finite-element method for solving the dynamic responses of the pipeline system in nuclear reactors. Olson and Jamison [8] used the nonlinear finite-element method to predict the response of elastic PCF. Lee and Oh [9] developed a spectral element model of the pipeline. The method provides more accuracy than the classical finite-element model. Wang and Bloom [10] developed a spatial finite-difference scheme for the stability analysis of submerged and inclined concentric PCF. Naguleswaran and Williams [11] adopted Rayleigh–Ritz and Fourier series solutions to study the lateral vibration of several common constrained PCF with consideration of axial tension and internal pressure. The dynamic properties of PCF are also investigated considering different conditions. Tang et al. [12] applied the multiple scales method to study the fractional dynamics of fluid-conveying pipes made of polymer-like materials. Mnassri and Baroudi [13] developed a theoretical method for the three-dimensional modal analysis of compressible fluid within pipes. The method can be used for defect detection. Zhou et al. [14] studied axially functional cantilevered PCF and analyzed the effects of the

elastic modulus gradient and density gradient on the critical flow velocity for flutter instability. Oke and Khulief [15] discussed the vibration behavior of a composite PCF having internal surface damage.

The mechanisms discovered in PCF have been gradually applied to other fields. By studying the lift effects of fluid force of a cantilevered elastic pipe for conveying fluid, Texier and Dorbolo [16] tried to introduce motion in soft robotics. The Coriolis effect in a Coriolis mass flow meter under lateral vibration was simulated by the finite-element method based on Timoshenko beam theory [17]. Recently, the extended dynamic models were applied to study the axially moving pipe [18–20] and helical tube conveying fluid [21]. Applications of the theory of PCF are not only limited to traditional pipes but also limited to micropipes and nanotubes conveying fluid [22–27] and even to the novel pipe composed of two different materials [28].

In practice, a pipeline usually works in the vibration environment. For instance, the aviation fuel pipeline lays on an aircraft engine, airborne pipes, and other fluid machinery equipment. In such a situation, the pipe supports are in the moving state. It may lead to constraints loosening, pipe fatigue failure, and/or leakage under such circumstances. In this study, the characteristics of dynamic response of PCF are investigated with consideration of both coupling effect between fluid and pipe and the external moving supports. Firstly, the dynamic equation for the pipe constrained by moving supports is deduced by the Newtonian method after finding the acceleration of fluid elements in Section 1. Secondly, by virtue of the Galerkin method, in Section 2, the discrete dynamic model is built and the fourth-order Runge–Kutta method is employed for numerical analysis. Finally, the influences of fluid velocity and the movement frequency of supports on the dynamic response of pipe are investigated in Section 3. The pipes with common boundaries, such as pinned-pinned, clamped-pinned, and clamped-clamped pipes, are discussed, respectively. In Section 4, some conclusions are drawn.

2. Dynamic Equation of PCF with Lateral Moving Supports

The diagram of PCF with lateral moving supports is shown in Figure 1. The global inertial reference frame is XOY with unit vectors $\mathbf{I}$ and $\mathbf{J}$. The moving reference frame xoy is attached to the supports, with unit vectors $\mathbf{i}$ and $\mathbf{j}$, lateral velocity v_0, and lateral acceleration a_0. The lateral deflection w is measured in the local frame xoy.

The acceleration of the fluid element, shown in Figure 2, is essential for derivation of the dynamic equation of PCF by the Newtonian method. Here, we introduce another moving reference frame $x'o'y'$ with unit vectors $\mathbf{i}'$ and $\mathbf{j}'$, which is attached to the pipe element. Parameters φ and ρ denote the slope angle of the pipe cross section and the curvature radius of the deformed pipe element, respectively. Without considering variation along radial direction, the acceleration of the fluid element can be represented by the acceleration of the fluid particle at the point O'.

Using the composition theorem in dynamics [29], the acceleration of the fluid element can be written as follows:

$$\mathbf{a}_\mathrm{f} = \mathbf{a}_\mathrm{r} + \mathbf{a}_\mathrm{e} + 2\boldsymbol{\omega} \times \mathbf{V}, \tag{2}$$

where $\mathbf{a}_\mathrm{r}$ is the relative acceleration, i.e., the fluid acceleration relative to the reference frame $x'o'y'$, and convected acceleration $\mathbf{a}_\mathrm{e}$ is the acceleration of the point O' fixed on the reference frame $x'o'y'$ relative to the inertial reference frame XOY. $\boldsymbol{\omega}$ denotes the angular velocity of the pipe cross section, that is $\boldsymbol{\omega} = (d\varphi/dt)\mathbf{k}'$, in which $\mathbf{k}'$ is the unit vector perpendicular to plane XOY outwardly. $\mathbf{V}$ is the velocity of fluid in the pipe, that is, $\mathbf{V} = V\ \mathbf{i}'$.

The terms in Equation (2) can be expressed as follows [1]:

$$\begin{aligned}
\mathbf{a}_\mathrm{r} &= \frac{dV}{dt}\mathbf{i}' - \frac{V^2}{\rho}\mathbf{j}', \\
\mathbf{a}_\mathrm{e} &= \frac{\partial^2 \delta}{\partial t^2}\mathbf{i} + \left(a_0 + \frac{\partial^2 w}{\partial t^2}\right)\mathbf{j} \simeq \left(a_0 + \frac{\partial^2 w}{\partial t^2}\right)\mathbf{j}, \\
2\boldsymbol{\omega} \times \mathbf{V} &= 2V\frac{d\varphi}{dt}\mathbf{k}' \times \mathbf{i}' = 2V\frac{\partial^2 w}{\partial s \partial t}\mathbf{j}',
\end{aligned} \tag{3}$$

where δ is the longitudinal displacement that is one order smaller than the lateral deflection w and can be neglected.

Substituting Equation (3) and $1/\rho = -(\partial^2 w/\partial s^2)/((1 + (\partial w/\partial s)^2)^{3/2}) \approx -\partial^2 w/\partial s^2$ into Equation (2), we have

$$\mathbf{a}_\mathrm{f} = \frac{dV}{dt}\mathbf{i}' + \left(2V\frac{\partial^2 w}{\partial s \partial t} + V^2\frac{\partial^2 w}{\partial s^2}\right)\mathbf{j}' + \left(a_0 + \frac{\partial^2 w}{\partial t^2}\right)\mathbf{j}. \tag{4}$$

Equation (4) can be further simplified once the transformation relationship between unit vectors $\mathbf{i}'$, $\mathbf{j}'$ and $\mathbf{i}$, $\mathbf{j}$ is given. As the pipe has small deformation, the transformation can be expressed as follows:

$$\begin{pmatrix} \mathbf{i}' \\ \mathbf{j}' \end{pmatrix} = \begin{pmatrix} \cos\varphi & \sin\varphi \\ -\sin\varphi & \cos\varphi \end{pmatrix}\begin{pmatrix} \mathbf{i} \\ \mathbf{j} \end{pmatrix} \approx \begin{pmatrix} 1 & \dfrac{\partial w}{\partial s} \\ -\dfrac{\partial w}{\partial s} & 1 \end{pmatrix}\begin{pmatrix} \mathbf{i} \\ \mathbf{j} \end{pmatrix}. \tag{5}$$

Substituting Equation (5) into Equation (4) and neglecting the second/higher order of infinitesimal, the expression of fluid acceleration yields

$$\mathbf{a}_\mathrm{f} = \frac{dV}{dt}\mathbf{i} + \left(\frac{dV}{dt}\frac{\partial w}{\partial s} + 2V\frac{\partial^2 w}{\partial s \partial t} + V^2\frac{\partial^2 w}{\partial s^2} + \frac{\partial^2 w}{\partial t^2} + a_0\right)\mathbf{j}. \tag{6}$$

If the pipe contains steady fluid and is nonextendable along axial direction, i.e., $s \approx x$ and $dV/dt = 0$, Equation (6) can be simplified further as follows:

$$\mathbf{a}_\mathrm{f} = \left(2V\frac{\partial^2 w}{\partial x \partial t} + V^2\frac{\partial^2 w}{\partial x^2} + \frac{\partial^2 w}{\partial t^2} + a_0\right)\mathbf{j}. \tag{7}$$

After obtaining the fluid acceleration, the dynamic equation can be deduced by the Newtonian method. The free body diagram of a pipe element is shown in Figure 3, where

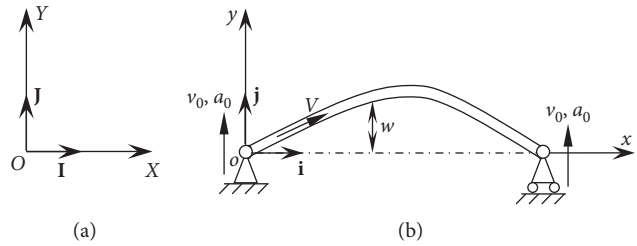

Figure 1: PCF with lateral moving supports.

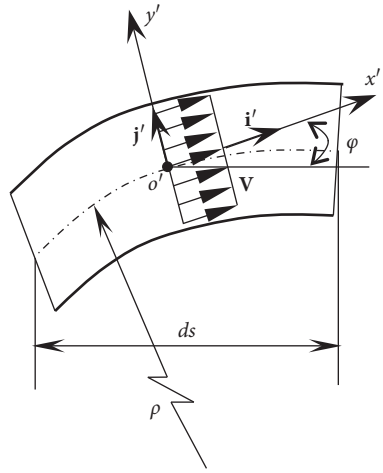

Figure 2: Fluid and pipe element.

Q and M are the transverse shear force and bending moment. The pipe contains fluid with pressure $\overline{p}$ and flow area A. m_f and m_p are the masses of fluid and pipe per length. The inertia force on the fluid and pipe elements is labeled as F_{If} and F_{Ip}, respectively. Hence, the lateral vibration equation of PCF can be formulated as follows:

$$\frac{\partial Q}{\partial x} - \overline{p}A\frac{\partial^2 w}{\partial x^2} = F_{If} + F_{Ip} = m_f a_f + m_p\left(a_0 + \frac{\partial^2 w}{\partial t^2}\right). \quad (8)$$

Substituting Equation (7) into Equation (8) and using the relationship between the shear force and bending moment, i.e., $(\partial Q/\partial x) = -(\partial^2 M/\partial x^2) = -(\partial^2/\partial x^2)(EI(\partial^2 w/\partial x^2))$, the lateral vibration equation is finally expressed as follows:

$$EI\frac{\partial^4 w}{\partial x^4} + \left(m_f V^2 + \overline{p}A\right)\frac{\partial^2 w}{\partial x^2} + 2m_f V\frac{\partial^2 w}{\partial x \partial t} + \left(m_f + m_p\right)\frac{\partial^2 w}{\partial t^2} = -\left(m_f + m_p\right)a_0. \quad (9)$$

When the supports vibrate harmonically, e.g., $A_0 \sin \omega_0 t$, the acceleration reads $a_0 = -A_0\omega_0^2 \sin \omega_0 t$, and the dynamic equation becomes

$$EI\frac{\partial^4 w}{\partial x^4} + \left(m_f V^2 + \overline{p}A\right)\frac{\partial^2 w}{\partial x^2} + 2m_f V\frac{\partial^2 w}{\partial x \partial t} + \left(m_f + m_p\right)\frac{\partial^2 w}{\partial t^2} = \left(m_f + m_p\right)A_0\omega_0^2 \sin \omega_0 t. \quad (10)$$

For convenience, the following dimensionless parameters are introduced to obtain the dimensionless form of Equation (10):

$$\begin{aligned} \eta &= \frac{w}{L}, \\ \xi &= \frac{x}{L}, \\ u &= \left(\frac{M}{EI}\right)^{1/2} LV, \\ P &= \frac{\overline{p}A}{EI}L^2, \\ \beta &= \left(\frac{m_f}{m_f + m_p}\right)^{1/2}, \\ \tau &= \left(\frac{EI}{m_f + m_p}\right)^{1/2}\frac{t}{L^2}, \\ \omega &= \left(\frac{m_f + m_p}{EI}\right)^{1/2}\omega_0 L^2, \\ \gamma &= \frac{A_0}{L}, \end{aligned} \quad (11)$$

where L is the length of the pipe.

Finally, the dimensionless form of Equation (10) becomes

$$\frac{\partial^4 \eta}{\partial \xi^4} + \left(u^2 + P\right)\frac{\partial^2 \eta}{\partial \xi^2} + 2\beta^{1/2}u\frac{\partial^2 \eta}{\partial \xi \partial \tau} + \frac{\partial^2 \eta}{\partial \tau^2} = \gamma\omega^2 \sin \omega\tau. \quad (12)$$

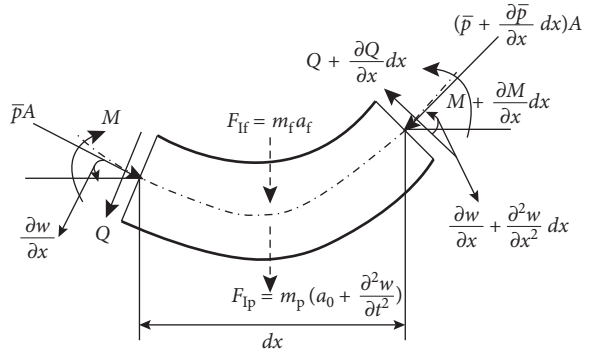

Figure 3: Free body diagram of a pipe element.

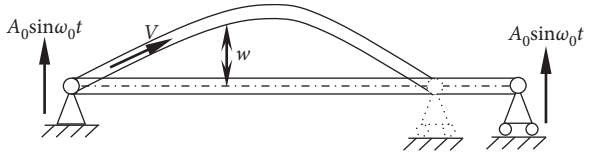

Figure 4: Pinned-pinned PCF.

3. Galerkin Discretization

The Galerkin method is applied to deal with the partial differential equation, and the dimensionless lateral deflection is represented as follows:

$$\eta(\xi, \tau) \simeq \sum_{i=1}^{N} \phi_i(\xi) q_i(\tau), \tag{13}$$

where $\phi_i(\xi)$ are the comparison functions and satisfy the boundary condition of the pipe and $q_i(\tau)$ are the generalized coordinates of the discretized pipe structure.

Substituting Equation (13) back into Equation (12) and minimizing the residual value, one will obtain the following discrete form of dynamic equation:

$$\mathbf{M}\ddot{\mathbf{q}} + \mathbf{C}\dot{\mathbf{q}} + \mathbf{K}\mathbf{q} = \mathbf{F}, \tag{14}$$

where $\mathbf{M}$, $\mathbf{C}$, $\mathbf{K}$, and $\mathbf{F}$ are the matrices of mass, damping, stiffness, and external load, respectively. Meanwhile, $\dot{\mathbf{q}}$ and $\ddot{\mathbf{q}}$ are the generalized velocity and acceleration.

The specific expressions of the elements of above matrices are as follows:

$$\begin{aligned} M_{ij} &= \int_0^1 \phi_i(\xi)\phi_j(\xi)\,d\xi, \\ C_{ij} &= 2\beta^{1/2}u \int_0^1 \phi_i'(\xi)\phi_j(\xi)\,d\xi, \\ K_{ij} &= \int_0^1 \left[\phi_i''''(\xi) + \left(u^2 + P\right)\phi_i''(\xi)\right]\phi_j(\xi)\,d\xi, \\ F_j &= \int_0^1 \gamma\omega^2 \sin\omega\tau\phi_j(\xi)\,d\xi, \end{aligned} \tag{15}$$

where $()' = \partial()/\partial x$.

The fourth-order Runge–Kutta method is employed to solve Equation (14) by changing the equation into the following form:

$$\dot{\mathbf{Y}}(\tau) = \mathbf{A}\mathbf{Y}(\tau) + \mathbf{P}(\tau), \tag{16}$$

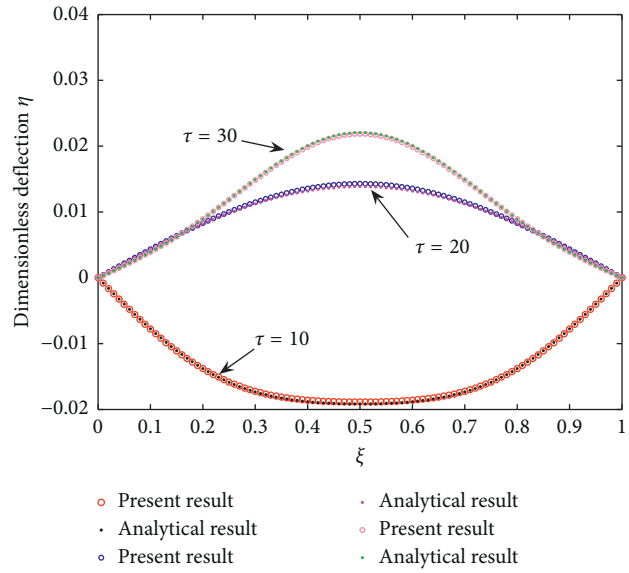

Figure 5: Comparison of deflection of the pinned-pinned pipe by two methods.

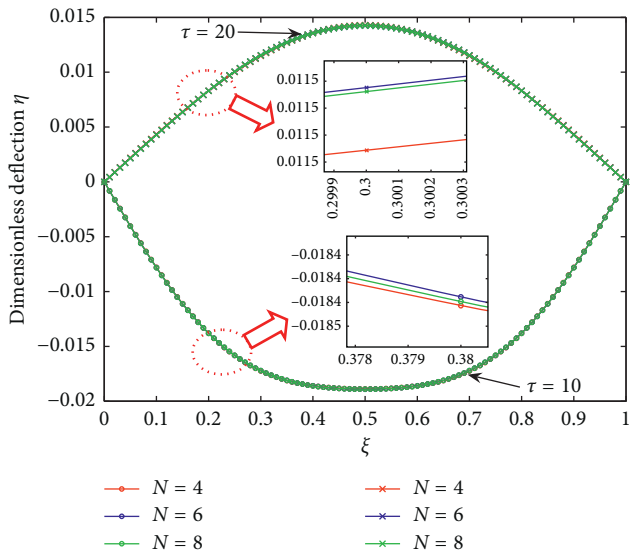

Figure 6: Comparison of deflections of the pinned-pinned pipe with different N.

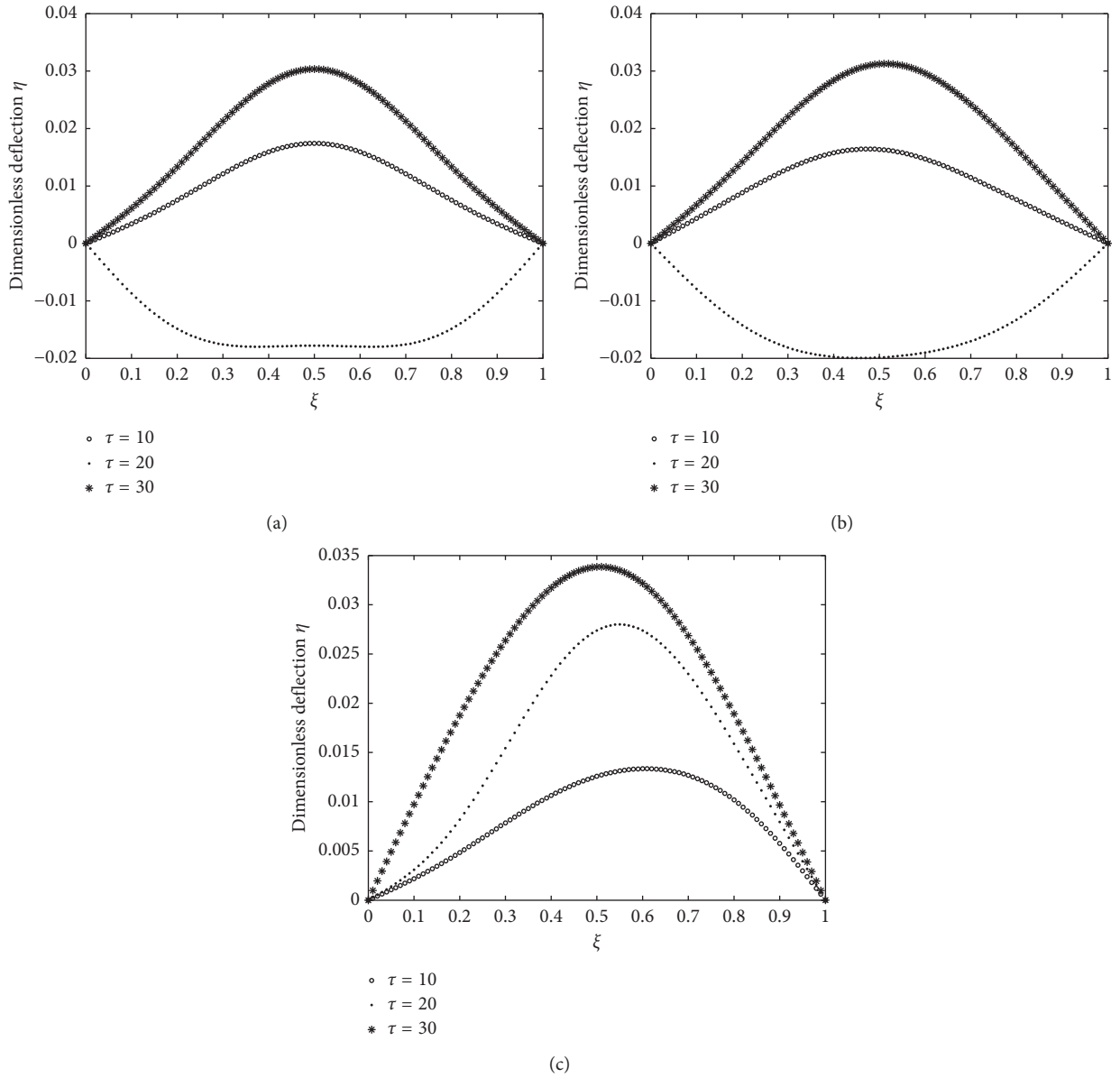

Figure 7: The deflections of the pinned-pinned pipe with different fluid velocities: (a) $u = 0$; (b) $u = 1$; (c) $u = 2$.

where $\mathbf{Y}(\tau) = \begin{pmatrix} \mathbf{q}(\tau) \\ \dot{\mathbf{q}}(\tau) \end{pmatrix}$, $\mathbf{A} = \begin{pmatrix} \mathbf{0}_{N\times N} & \mathbf{I}_{N\times N} \\ -\mathbf{M}^{-1}\mathbf{K} & -\mathbf{M}^{-1}\mathbf{C} \end{pmatrix}$, and $\mathbf{P}(\tau) = \begin{pmatrix} \mathbf{0}_{N\times 1} \\ \mathbf{M}^{-1}\mathbf{F} \end{pmatrix}$. $\mathbf{I}_{N\times N}$ is the N-ordered identity matrix.

In numerical analysis, the dimensionless time step is set as $\Delta\tau = 0.002$ and the initial conditions are $\mathbf{q}(\tau) = \mathbf{0}$ and $\dot{\mathbf{q}}(\tau) = \mathbf{0}$. According to Paidoussis and Semler [30], Wang et al. [31], and Ni et al. [20], the convergence can be guaranteed when the order of the Galerkin truncation error of Equation (13) satisfies $N \geq 4$. In this study, we choose $N = 8$ for the following analysis.

4. Examples

In the examples, the following parameters are chosen for PCF: elastic modulus of the pipe material $E = 68$ GPa, the Poisson ratio $\mu = 0.33$, and the density $\rho_p = 2700\,\text{kg}\cdot\text{m}^{-3}$. The outer and inner diameters of the pipe are $D = 46$ mm and $d = 40$ mm, respectively. The pipe length is $L = 2$ m. The fluid density is $\rho_f = 870\,\text{kg}\cdot\text{m}^{-3}$, and the mean inner pressure $\overline{p} = 2$ MPa. The supports are moved harmonically, i.e., $A_0 \sin(\omega_0 t)$, with the amplitude of $A_0 = 0.005$ m and angular frequency of $\omega_0 = 300\pi$ rad s^{-1}.

Table 1: The dimensionless natural frequencies of the pinned-pinned PCF.

u	ω			
	ω_1	ω_2	ω_3	ω_4
0	9.05	38.68	88.04	157.13
1	8.44	38.22	87.61	156.71
2	6.37	36.81	86.31	155.46

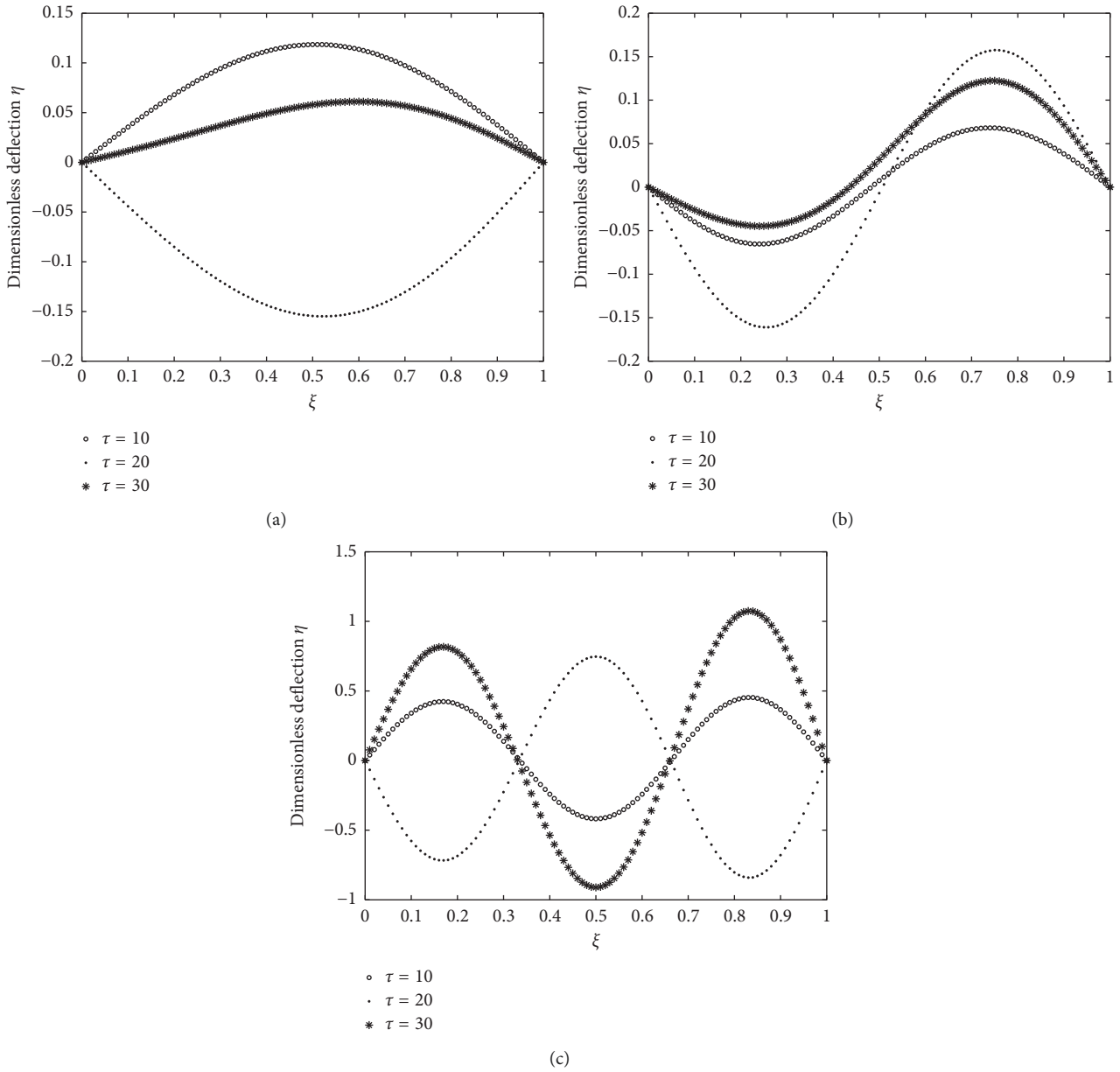

FIGURE 8: The resonance responses of the pinned-pinned PCF with $u = 1$ under different supports moving frequencies: (a) $\omega = 8.44$; (b) $\omega = 38.22$; (c) $\omega = 87.61$.

4.1. The Pinned-Pinned PCF. In beam theory, the comparison function for the pinned-pinned pipe, shown in Figure 4, is $\phi_i(\xi) = \sin i\pi\xi$. To show the effectiveness of the proposed method, we compare the results obtained by both the analytical mode superposition method for classical beam problems and the proposed method. For a solid beam, it can be considered as a PCF with zero velocity of fluid ($u = 0$) and without inner pressure ($\overline{p} = 0$). Comparison of the results will be carried out when $u = 0$ and $\overline{p} = 0$. It is easy to find out Equation (12) draws the state of a pipe with stationary supports and subjected to uniform load $p(\xi,\ \tau) = \gamma\omega^2 \sin\omega\tau$. In this case, based on the mode superposition method and beam theory [32], the lateral deflection of the pipe can be expressed as follows:

$$\eta(\xi,\ \tau) = \sum_i \phi_i(\xi) q_i(\tau). \tag{17}$$

Considering the uniform external load $p(\xi,\ \tau) = \gamma\omega^2 \sin\omega\tau$ and initial condition, i.e., $\eta(\xi,\ 0) = \dot{\eta}(\xi,\ 0) = 0$, the generalized coordinate can be expressed analytically [32] as follows:

$$\begin{aligned} q_i(\tau) &= \left(1 - (-1)^i\right) \frac{1}{\omega_i} \frac{2\gamma\omega^2}{i\pi} \int_0^\tau \sin\omega\zeta \sin\omega_i(\tau - \zeta)\, d\zeta \\ &= \frac{2\gamma\omega^2}{i\pi} \frac{\left(1 - (-1)^i\right)}{\omega_i^2 - \omega^2} \left(\sin\omega\tau - \frac{\omega}{\omega_i} \sin\omega_i\tau\right), \end{aligned} \tag{18}$$

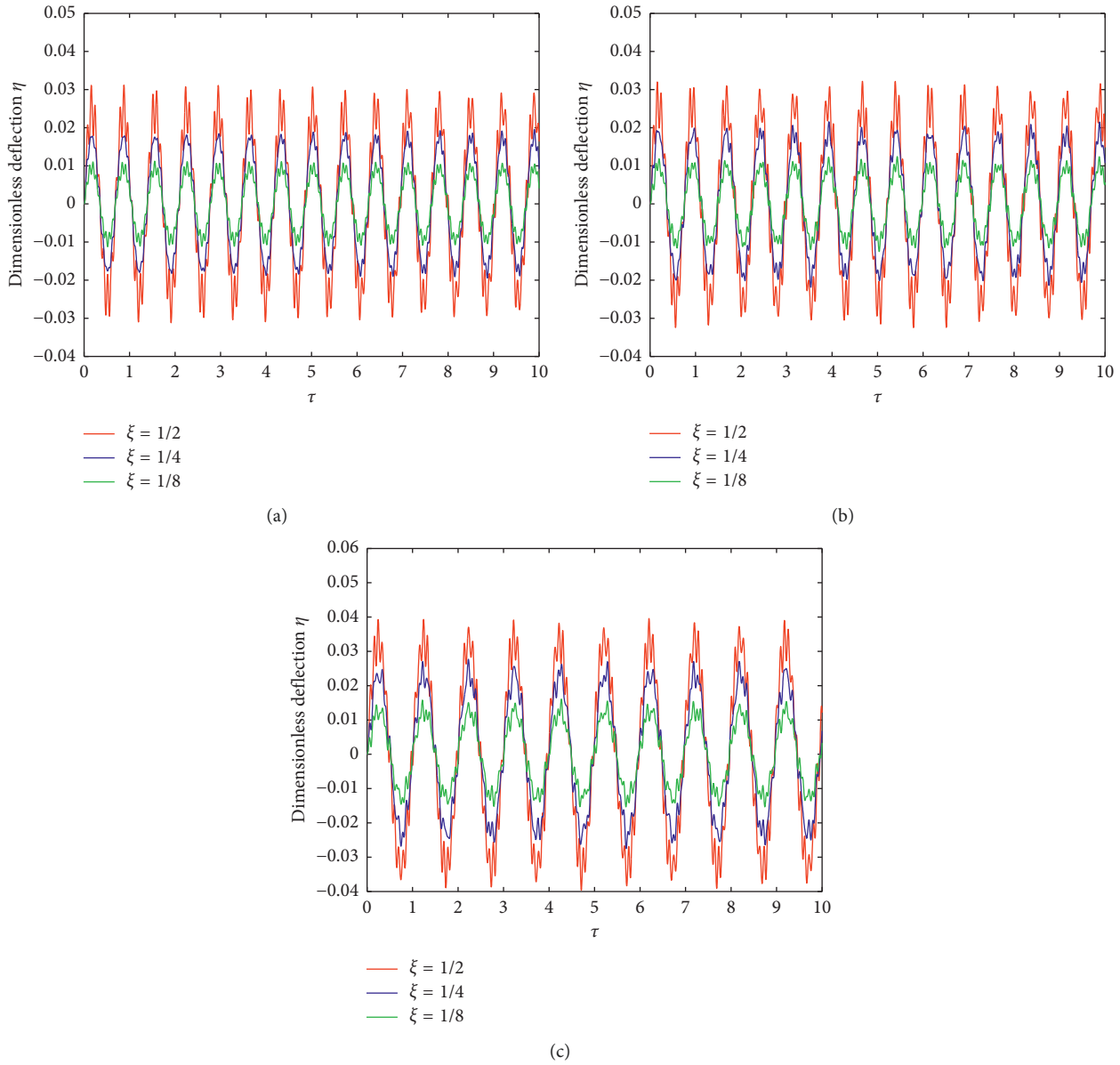

Figure 9: History curves of deflection at different locations on the pinned-pinned pipe having different fluid velocities: (a) $u = 0$; (b) $u = 1$; (c) $u = 2$.

where ω_i is the ith natural frequency of the pinned-pinned pipe with stationary fluid and zero inner pressure.

Now, the analytical solution for the pipe deflection can be obtained by substituting Equation (18) into Equation (17). We find that the results obtained by the mode superposition method are stable when $i \geq 3$. Hence, we set $i = 4$ for the comparison. The results calculated by the two methods (Figure 5) match each other very well. Hence, the validation of the present method is verified.

We choose three different truncations of Equation (13), with $N = 4$, 6, and 8, in finding the responses of the pinned-pinned pipe. As demonstrated in Figure 6, the three results are almost the same and converge to the analytical solutions as long as $N \geq 4$.

The lateral deflections of the pinned-pinned pipe with three different fluid velocities ($u = 0$, $u = 1$, and $u = 2$) at three different moments ($\tau = 10$, $\tau = 20$, and $\tau = 30$) are involved in discussion in this paper. The detailed results are illustrated in Figure 7.

The three modes of deflection curves in Figure 7 are different in each case. Meanwhile, the deflection curves in Figures 7(b) and 7(c) are asymmetric due to flow of fluid within the beam. It is easy to find out in Figure 7 that the deflections gradually increase with fluid velocity. This implies that the rigidity of the pipe becomes lower when the fluid speed is higher. The effect also appears on the natural frequencies of the pipe with different fluid velocities. In this paper, the first four orders of natural frequency are calculated through the wave approach which was introduced by Li et al. [33, 34]. The results are listed in Table 1.

In practice, when the external vibration frequency is in coincidence with the natural frequencies of structures, then

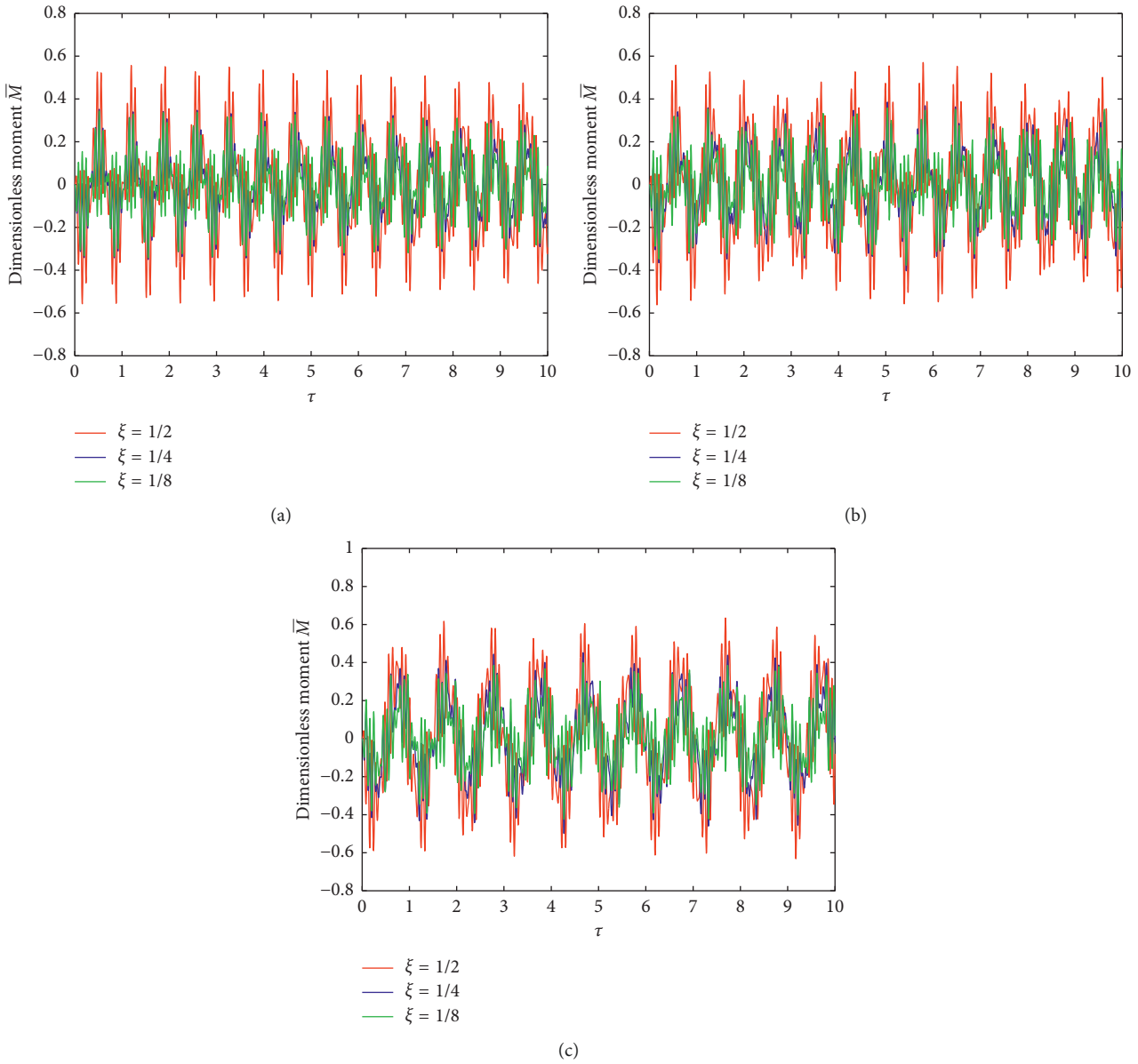

Figure 10: History curves of bending moment on the pinned-pinned pipe at different locations and having different fluid velocities: (a) $u = 0$; (b) $u = 1$; (c) $u = 2$.

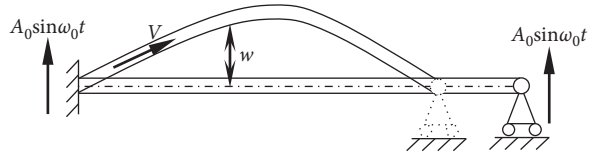

Figure 11: The model for a clamped-pinned PCF.

structural resonance will happen, and large deformation will be generated. To evaluate such an effect on pipe structures, we investigate the deflections of PCF with supports moving in the same frequencies as its natural frequencies.

For simplicity, the deflections of the pinned-pinned pipe with fluid velocity $u = 1$ are analyzed, and three cases with respect to the moving frequency of the supports, i.e., $\omega =$ 8.44, 38.22, and 87.61, are considered. Figure 8 shows the resonance responses in the three cases.

Table 2: The values of $\beta_i l$ for clamped-pinned PCF.

$\beta_1 l$	$\beta_2 l$	$\beta_3 l$	$\beta_4 l$
3.9266	7.0686	10.2102	13.3518

Compared with the results in Figure 7, the amplitudes of deflections in Figure 8 become much larger, especially when

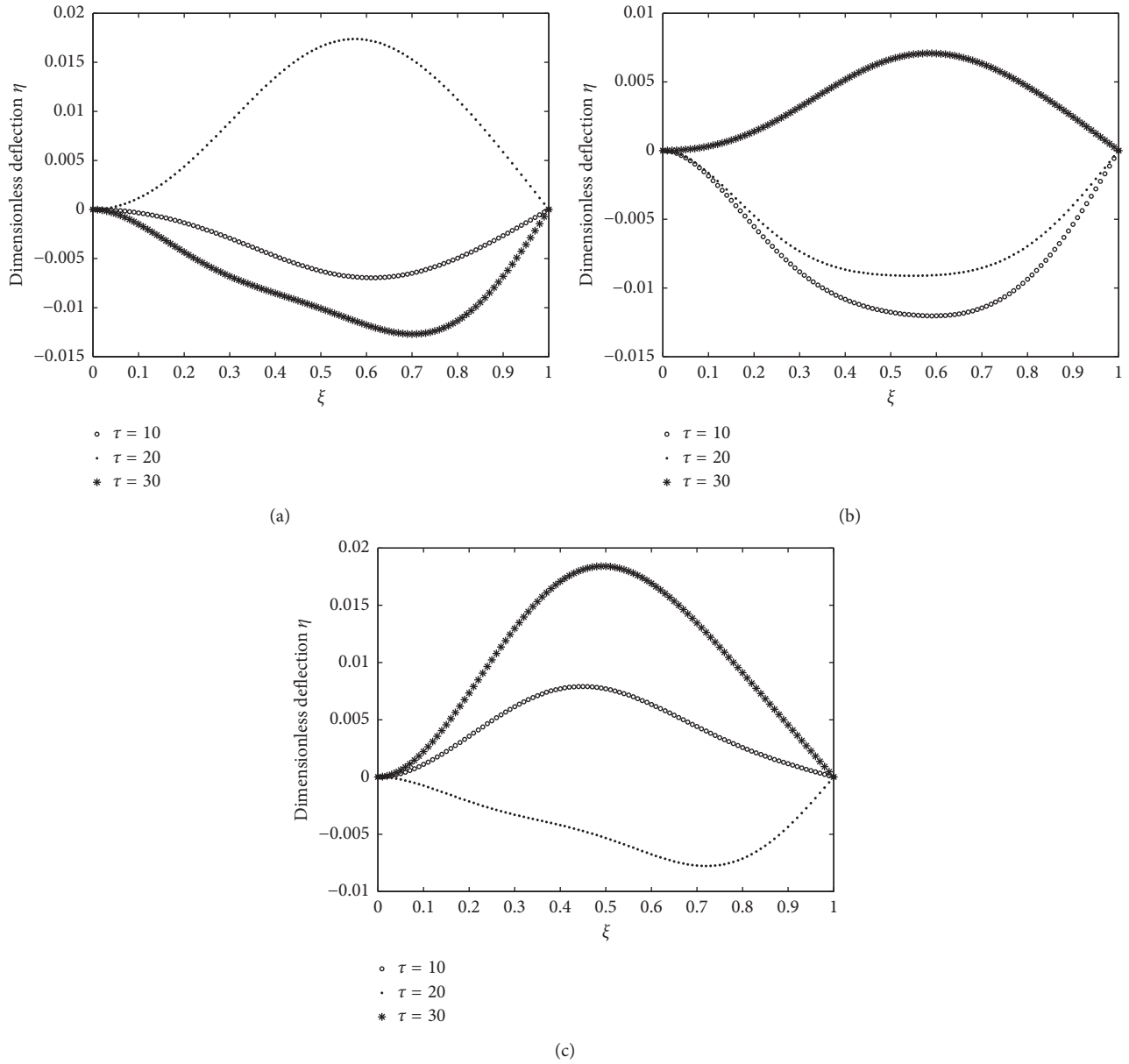

Figure 12: The deflection responses of the clamped-pinned pipe under different fluid velocities: (a) $u = 0$; (b) $u = 1$; (c) $u = 2$.

the supports moving frequency reaches the third natural frequency of PCF. At the times $\tau = 20$ and $\tau = 30$ in Figure 8(c), the largest amplitude of deflection appears near the right end of the pipe rather than at the center. The same phenomenon can be found in Figure 7(c).

We also obtain the history curves of pipe deflection at different locations ($\xi = 1/2$, $\xi = 1/4$, and $\xi = 1/8$) under different fluid velocities ($u = 0$, $u = 1$, and $u = 2$) (Figure 9).

Figure 9 suggests that the amplitude of deflection increases with the fluid velocity. The maximum deflection occurs at the center of the pipe. Deflection of a point becomes smaller when the point is closer to a pipe end. With the increase of fluid velocity, the response curves are gradually getting sparse. It implies that the response period becomes larger; i.e., the natural frequency is getting smaller.

Bending moment is another important dynamic response for the beam. Once it is obtained, the normal stress on the pipe cross section will be determined. Furthermore, the fatigue analysis can be conducted. From Equation (13), the expression of dimensionless bending moment becomes

$$\overline{M} = \frac{ML}{EI} = \frac{\partial^2 \eta}{\partial \xi^2}. \tag{19}$$

Figure 10 illustrates the history curves of bending moment on the pinned-pinned pipe at three different locations ($\xi = 1/2$, $\xi = 1/4$, and $\xi = 1/8$) with respect to three different fluid velocities ($u = 0$, $u = 1$, and $u = 2$).

In Figure 10(a), when $u = 0$, the bending moment at $\xi = 1/2$ is larger than those at $\xi = 1/4$ and $\xi = 1/8$, but the bending moments at $\xi = 1/4$ and $\xi = 1/8$ are different slightly. As the

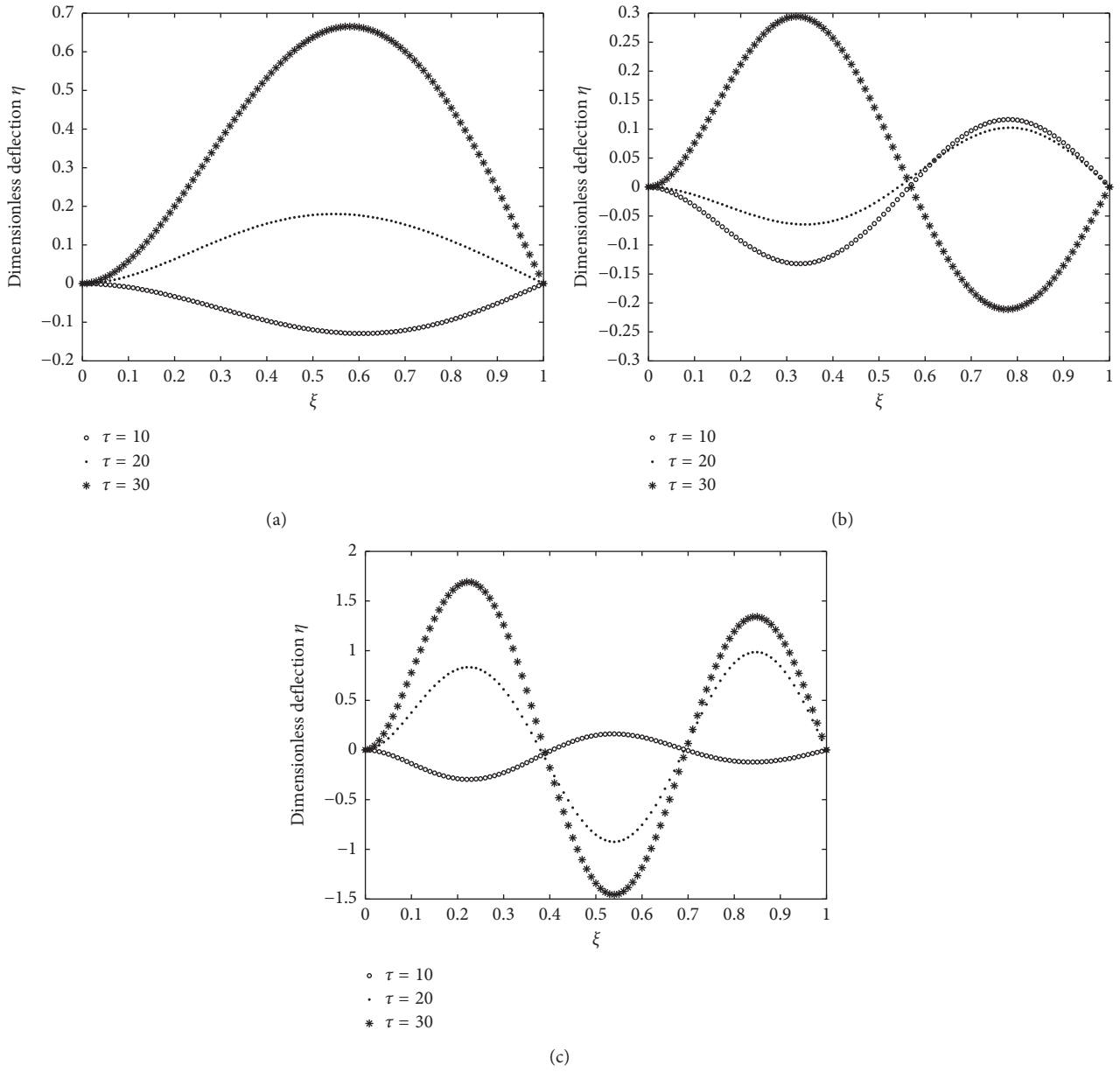

Figure 13: The resonance responses of the clamped-pinned pipe with $u = 1$ and different supports moving frequencies: (a) $\omega = 14.36$; (b) $\omega = 48.89$; (c) $\omega = 103.15$.

fluid velocity increases, the bending moments at the three locations increase, simultaneously. However, at $\xi = 1/4$ and $\xi = 1/8$, they tend to have a faster increase than that at location $\xi = 1/2$.

4.2. The Clamped-Pinned PCF. Another type of fluid-conveying pipe is the clamped-pinned pipe in Figure 11. Its comparison function [35] becomes

$$\phi_i(\xi) = \sin\beta_i\xi - \sinh\beta_i\xi + \alpha_i(\cosh\beta_i\xi - \cos\beta_i\xi), \quad (20)$$

where $\alpha_i = (\sin\beta_i l - \sinh\beta_i l)/(\cos\beta_i l - \cosh\beta_i l)$ and $\beta_i l \approx (i + 1/4)\pi$ when $i \geq 1$. The values of $\beta_i l$ are listed in Table 2 [35]. At three different times ($\tau = 10$, $\tau = 20$, and $\tau = 30$), the deflection responses of the pipe having three different fluid velocities ($u = 0$, $u = 1$, and $u = 2$) are illustrated in Figure 12.

Table 3: The first four orders of dimensionless natural frequencies of the clamped-pinned PCF.

u	ω			
	ω_1	ω_2	ω_3	ω_4
0	14.82	49.29	103.54	177.55
1	14.36	48.89	103.15	177.16
2	12.94	47.69	101.98	176.00

There is no symmetric mode in any case of Figure 12 due to the asymmetric supports. Deflection of the pipe does not vary monotonously with the fluid velocity. At time $\tau = 10$, with the increase of fluid velocity, the deflection first

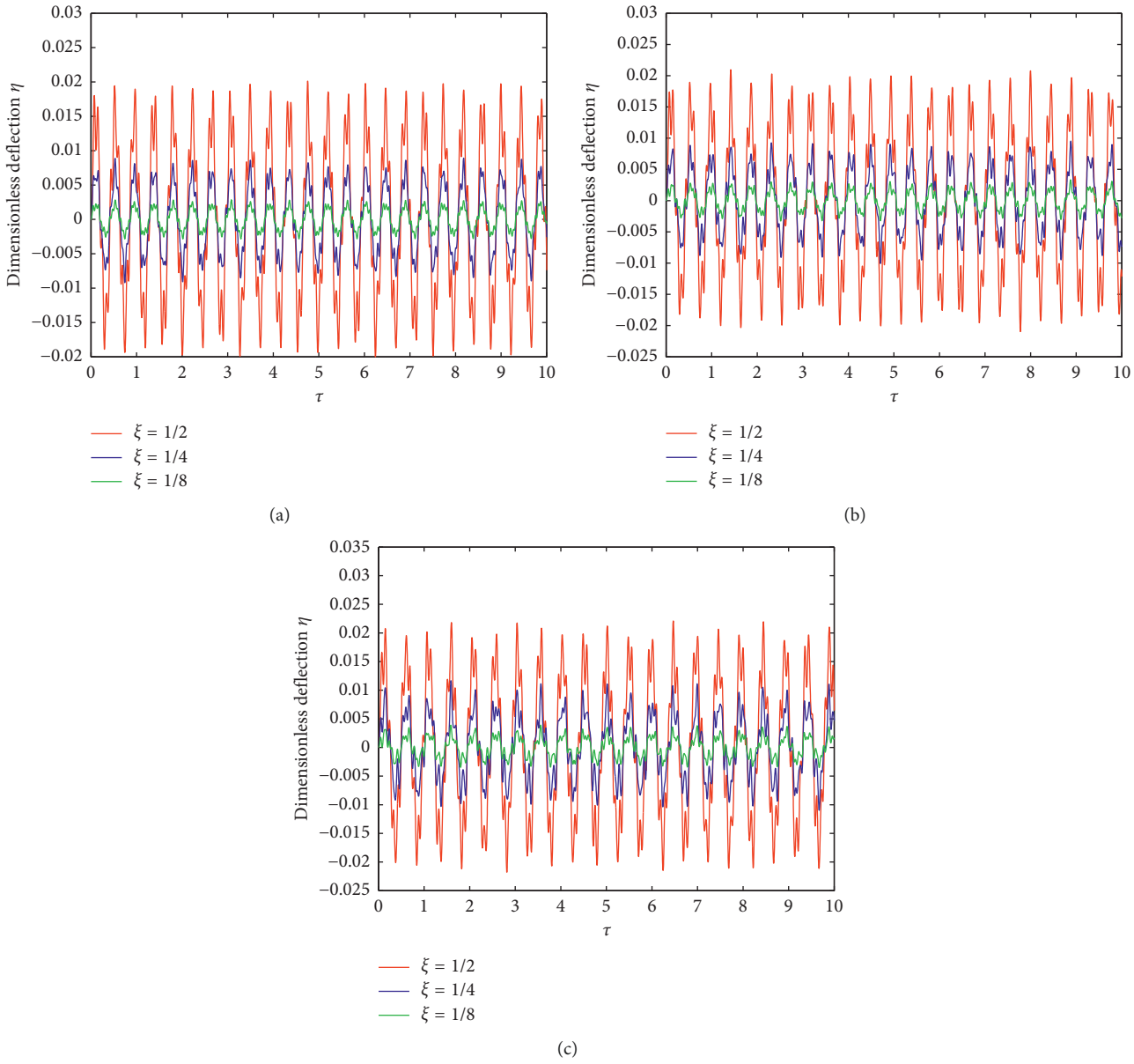

FIGURE 14: History curves of the deflection of the clamped-pinned pipe at different locations and having different fluid velocities: (a) $u = 0$; (b) $u = 1$; (c) $u = 2$.

increases and then turns to decrease. However, at time $\tau = 20$, the deflection always decreases. At time $\tau = 30$, the deflection firstly decreases and then increases.

The first four natural frequencies of the clamped-pinned PCF are calculated by the wave approach [33, 34] (Table 3). The resonance analysis with respect to fluid velocity $u = 1$ is also carried out when the supports moving frequencies ω_i are equal to 14.36, 48.89, and 103.15, respectively.

The deflection curves in Figures 13(a) and 13(c) are much larger than that in Figure 13(b), and the largest deflection appears in Figure 13(c). In other words, the resonance is very strong once the supports moving frequency equals the first or the third natural frequency of the pipe. The largest deflection occurs at the right side of the pipe center in Figure 13(a), whilst at the left side of the pipe center in Figures 13(b) and 13(c).

The history curves of the deflection of the clamped-pinned pipe conveying fluid at different locations ($\xi = 1/2$, $\xi = 1/4$, and $\xi = 1/8$) and having different fluid velocities ($u = 0$, $u = 1$, and $u = 2$) are illustrated in Figure 14.

It can also be observed that the deflections increase with the fluid velocity. Compared with the pinned-pinned pipe, however, the clamped-pined pipe has lower variation of deflection due to larger support stiffness at the clamped end of the clamped-pinned pipe, and the same fluid velocity produces smaller effect on the pipe deflection.

The history curves of bending moment on the clamped-pinned pipe in different cases are given in Figure 15. Figure 15 indicates that, in each case, the largest bending moment on the clamped-pinned pipe appears at $\xi = 1/2$, and this is the same as that of the pinned-pinned pipe. The bending moment at $\xi = 1/8$, however, is larger than that at $\xi = 1/4$, and this is

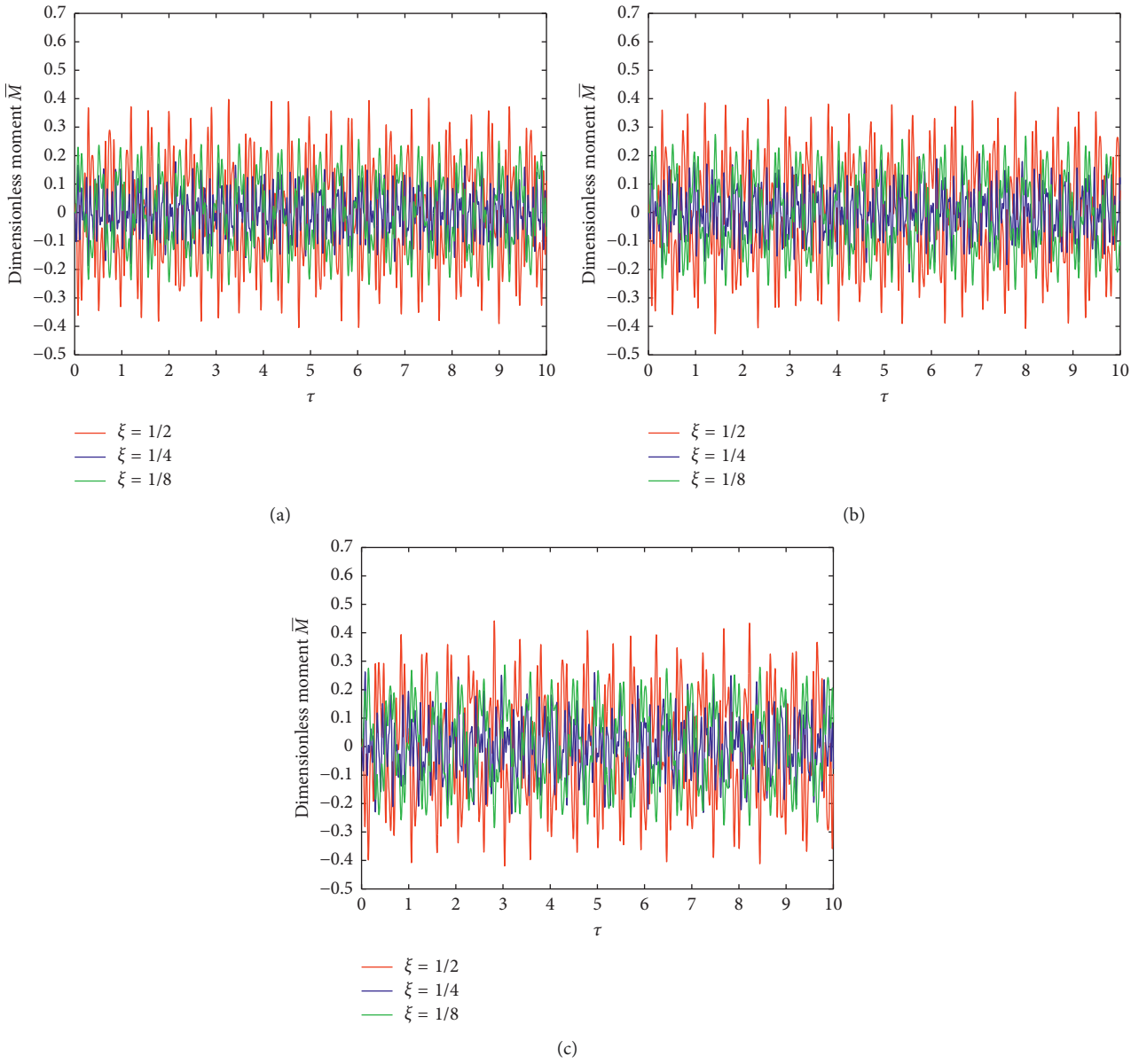

Figure 15: History curves of bending moment response for the clamped-pinned pipe at different locations and under different fluid velocities: (a) $u = 0$; (b) $u = 1$; (c) $u = 2$.

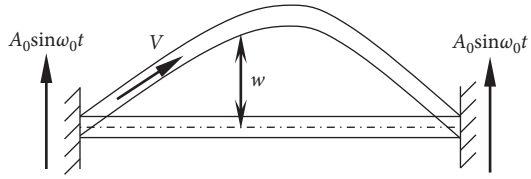

Figure 16: Schematic of a clamped-clamped PCF.

different from that of the pinned-pinned pipe. And the magnitude of bending moment on the clamped-pinned pipe is much lower than that of the pinned-pinned pipe.

4.3. The Clamped-Clamped PCF. The dynamic model for the clamped-clamped pipe, shown in Figure 16, is different from that for either the pinned-pinned pipe or the clamped-pinned pipe because the inextensible assumption is not suitable anymore. It is easy to find from Figure 16 that while vibration happens, the axial extension is inevitably permitted as the beam has transverse vibration. If so, an additional tensile force, which equals $T = 2\mu \overline{p} A_f$, should be induced on the cross section of the pipe [1]. Hence, the dynamic equation of the clamped-clamped PCF needs to be modified as follows:

Table 4: The values of $\beta_i l$ for the clamped-clamped PCF.

$\beta_1 l$	$\beta_2 l$	$\beta_3 l$	$\beta_4 l$
4.7300	7.8532	10.9956	14.1372

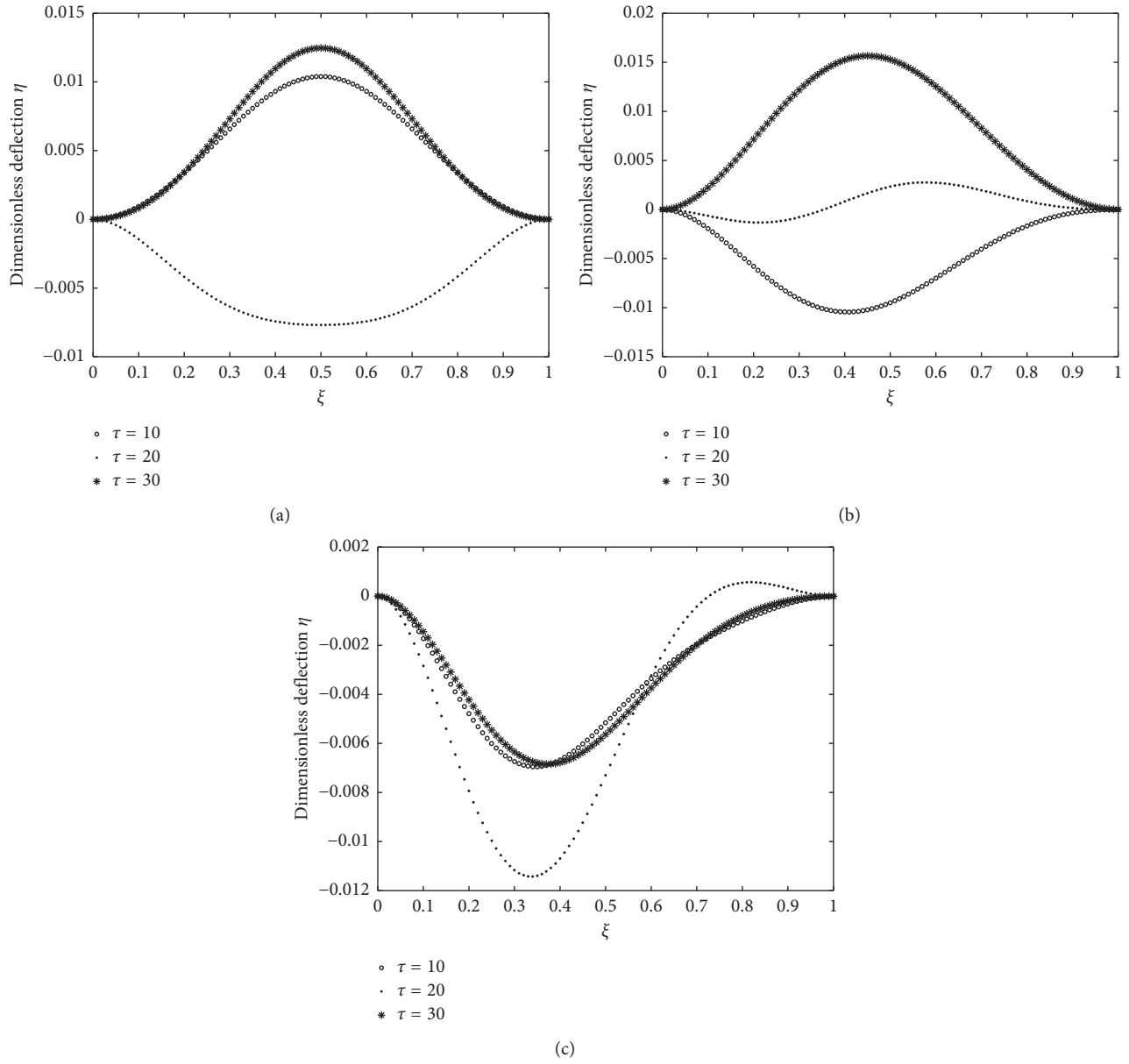

Figure 17: The deflections of the clamped-clamped pipe having different fluid velocities: (a) $u = 0$; (b) $u = 1$; (c) $u = 2$.

$$EI\frac{\partial^4 w}{\partial x^4} + \left[m_f V^2 + \overline{p}A(1-2\mu)\right]\frac{\partial^2 w}{\partial x^2} + 2m_f V\frac{\partial^2 w}{\partial x \partial t} + \left(m_f + m_p\right)\frac{\partial^2 w}{\partial t^2} = \left(m_f + m_p\right)A_0\omega_0^2 \sin\omega_0 t. \tag{21}$$

Correspondingly, the dimensionless form of Equation (21) can be written as follows:

$$\frac{\partial^4 \eta}{\partial \xi^4} + \left[u^2 + P(1-2\mu)\right]\frac{\partial^2 \eta}{\partial \xi^2} + 2\beta^{1/2}u\frac{\partial^2 \eta}{\partial \xi \partial \tau} + \frac{\partial^2 \eta}{\partial \tau^2} = \gamma\omega^2 \sin\omega\tau. \tag{22}$$

In the discrete form of Equation (14), only the stiffness matrix needs to be changed into the following form:

Table 5: The first four dimensionless natural frequencies of the clamped-clamped PCF.

u	ω			
	ω_1	ω_2	ω_3	ω_4
0	22.23	61.47	120.69	199.63
1	21.87	61.13	120.33	199.27
2	20.79	60.10	119.27	198.20

$$K_{ij} = \int_0^1 \left[\phi_i''''(\xi) + \left[u^2 + P(1-2\mu)\right]\phi_i''(\xi)\right]\phi_j(\xi)\,d\xi. \tag{23}$$

The comparison function of the clamped-clamped pipe is expressed as follows [35]:

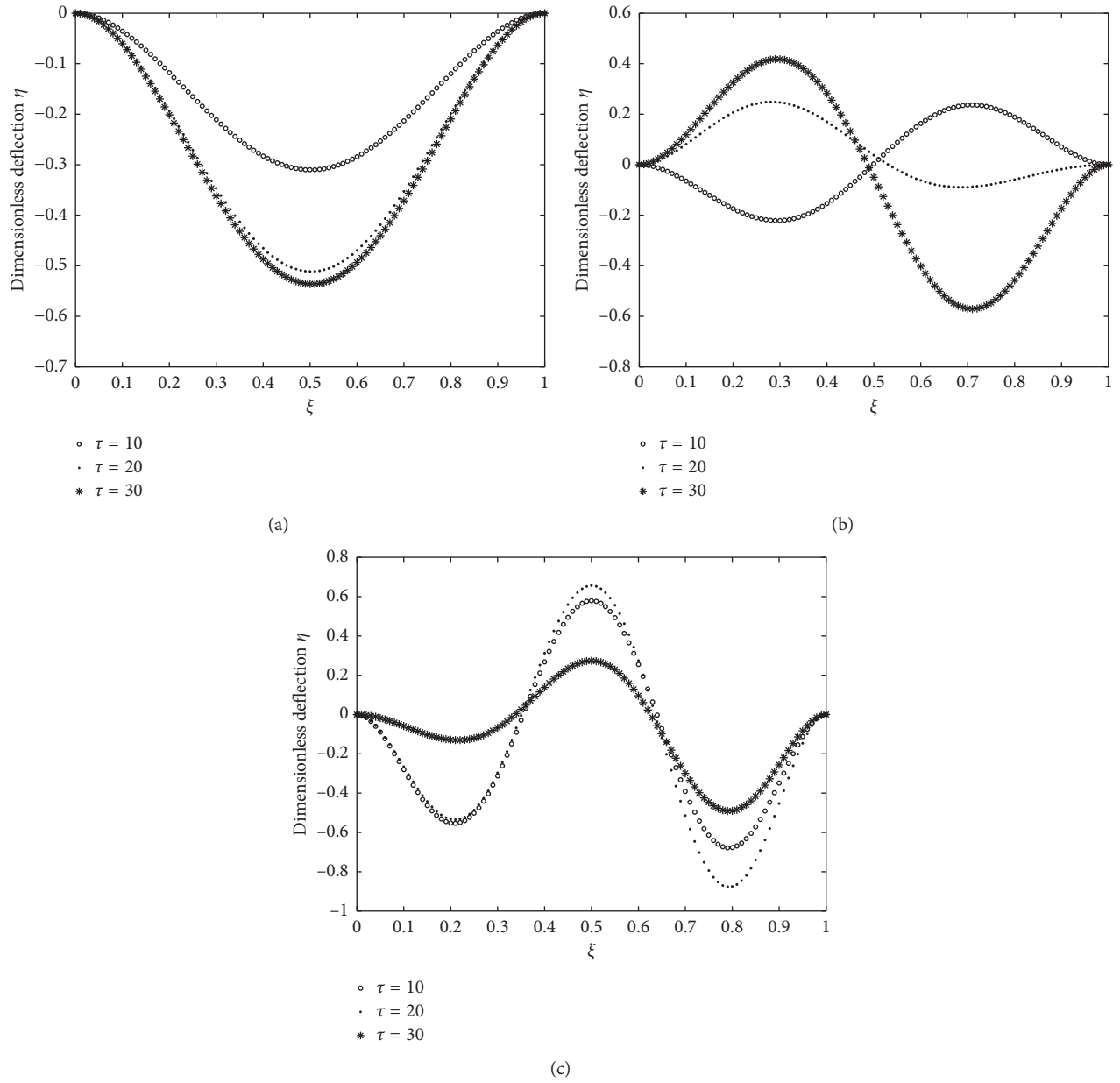

FIGURE 18: The resonance responses of the clamped-clamped pipe with $u = 2$ under different supports movement frequencies: (a) $\omega = 20.79$; (b) $\omega = 60.10$; (c) $\omega = 119.27$.

$$\phi_i(\xi) = \sinh\beta_i\xi - \sin\beta_i\xi + \lambda_i\left(\cosh\beta_i\xi - \cos\beta_i\xi\right), \quad (24)$$

where $\lambda_i = (\sinh\beta_i l - \sin\beta_i l)/(\cos\beta_i l - \cosh\beta_i l)$ and $\beta_i l \approx (i + 1/2)\pi$, when $i \geq 2$. The values of $\beta_i l$ are listed in Table 4. With different fluid velocities ($u = 0$, $u = 1$, and $u = 2$), the deflections of the clamped-clamped pipe at different moments ($\tau = 10$, $\tau = 20$, and $\tau = 30$) are shown in Figure 17.

The deflections of the clamped-clamped pipe are the smallest among the three types of pipes due to two reasons: one is the clamped-clamped pipe having the largest stiffness and the other is the existence of the axial tensile force on the cross section of the pipe. In Figures 17(a) and 17(b), the largest amplitudes are different slightly because of counteracting influences of fluid and the axial tensile force. In Figures 17(b) and 17(c), the maximum deflection occurs at the left side of the pipe center.

The first four orders of natural frequencies of the clamped-clamped PCF are listed in Table 5. In resonance analysis, the resonance responses with fluid velocity $u = 2$ and supports movement frequencies $\omega = 20.79$, 60.10, and 119.27 are considered. The detailed reflection curves are illustrated in Figure 18.

The strongest resonance appears at $\omega = 119.27$ and the weakest at $\omega = 60.10$. The deflection curves in Figure 18(a) are almost symmetric, which are different from that of either the pinned-pinned pipe or the clamped-pinned pipe. In Figures 18(b) and 18(c), the

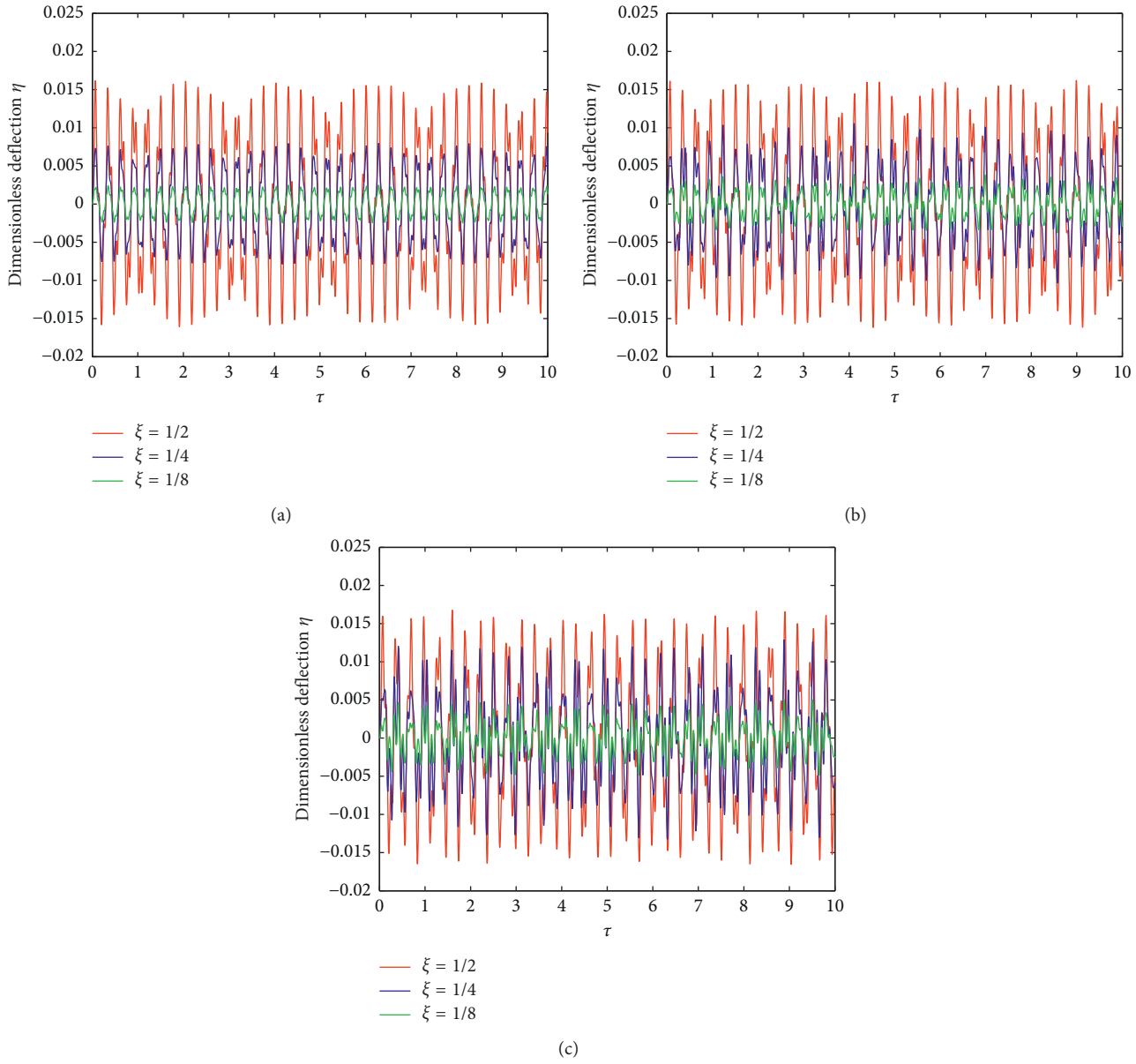

Figure 19: History curves of the deflection of the clamped-pinned pipe at different locations when having different fluid velocities: (a) $u = 0$; (b) $u = 1$; (c) $u = 2$.

maximum deflection appears at the right side of the pipe center.

Figure 19 gives the history curves of deflection of the clamped-clamped fluid-conveying pipe at different locations ($\xi = 1/2$, $\xi = 1/4$, and $\xi = 1/8$) when having different fluid velocities ($u = 0$, $u = 1$, and $u = 2$).

From Figure 19, one can find that the flexural rigidity of the pipe is weakened by flowing fluid. The influence of fluid on the pipe is lower than those on the other two pipes.

History curves of bending moment on the clamped-clamped fluid-conveying pipe are shown in Figure 20.

When the pipe is with stationary fluid, i.e., $u = 0$ (Figure 20(a)), the maximum bending moment appears at $\xi = 1/2$ and the minimum at $\xi = 1/4$. When the fluid velocity becomes $u = 1$ (Figure 20(b)), the bending moment at $\xi = 1/4$ tends to be identical to that at $\xi = 1/8$. When the fluid velocity reaches $u = 2$ (Figure 20(c)), the bending moment at $\xi = 1/4$ is higher than that at $\xi = 1/8$ and is almost the same as that at $\xi = 1/2$.

5. Concluding Remarks

The dynamic responses of three types of fluid-conveying pipes with lateral moving supports are investigated in this paper. The dynamic equations are deduced after obtaining the acceleration of fluid. The Galerkin method and fourth-order Runge–Kutta method are adopted in the numerical analysis. The responses with respect to deflection and bending moment are obtained considering different fluid

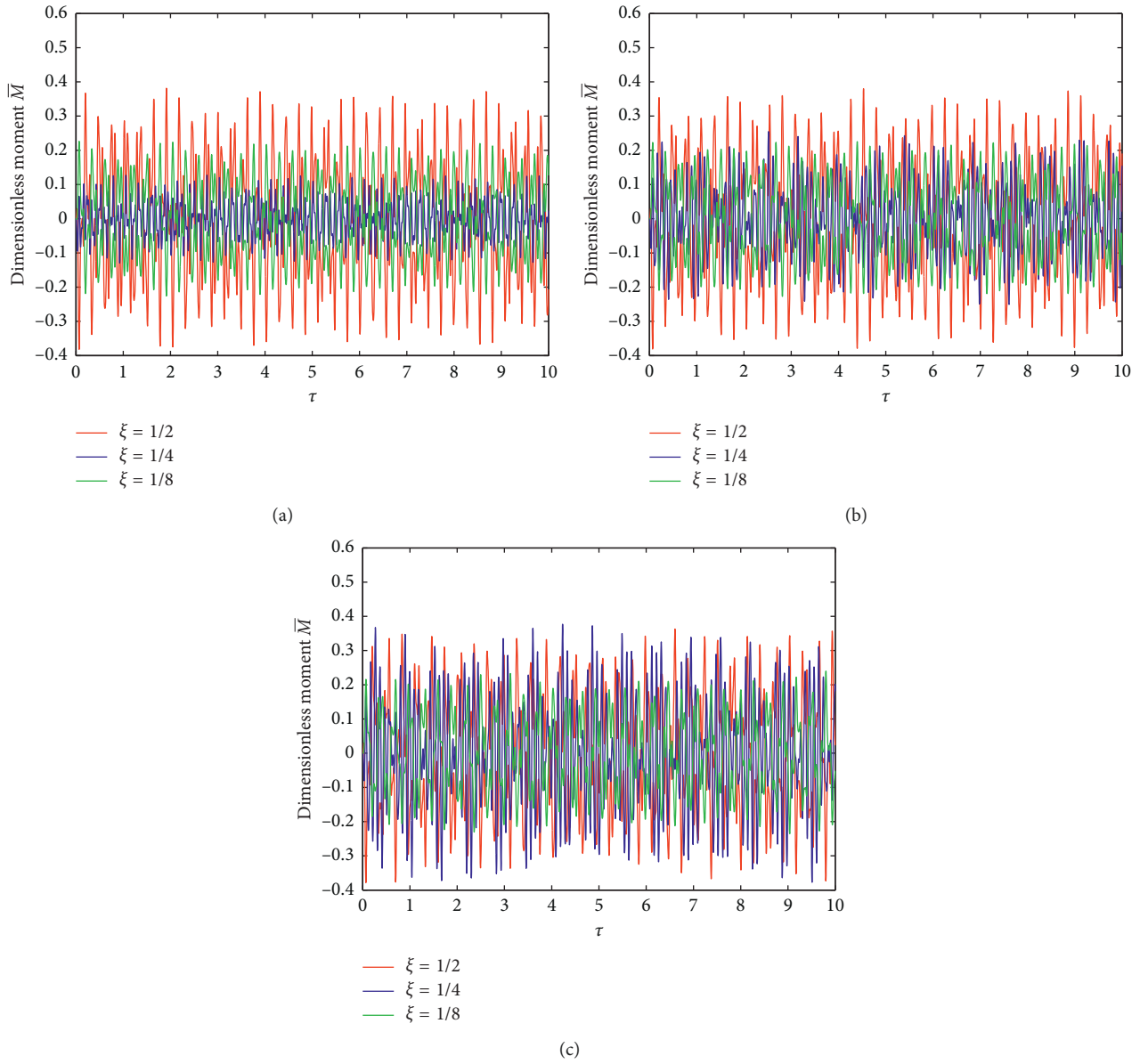

FIGURE 20: History curves of bending moment on the clamped-clamped pipe with different fluid velocities at different locations: (a) $u = 0$; (b) $u = 1$; (c) $u = 2$.

velocities. Some conclusions are drawn according to the numerical analysis:

(1) Both the deflection and bending moment responses increase with the fluid velocity.

(2) The largest bending moment on the pinned-pinned pipe appears at $\xi = 1/2$. The difference between the bending moments at $\xi = 1/4$ and $\xi = 1/8$ is slight, which is independent of the fluid velocity.

(3) The magnitudes of bending moment on the clamped-pinned and clamped-clamped pipes satisfy $\overline{M}(\xi = 1/2) > \overline{M}(\xi = 1/8) > \overline{M}(\xi = 1/4)$ when the fluid is in the stationary state. However, the bending moment at $\xi = 1/4$ increases sharply with the fluid velocity and tends to be identical to that at $\xi = 1/8$.

(4) Strong resonance will happen when the supports movement frequency equals the odd-ordered natural frequencies of the PCF.

Data Availability

The data used to support the findings of this study are available from the corresponding author upon request.

Conflicts of Interest

The authors declare that they have no conflicts of interest.

Acknowledgments

This work was supported by the National Natural Science Foundation of China (Grant No. 51505388). We appreciate Professor Kun Cai for his valuable suggestions and improvement in the language.

References

[1] M. P. Païdoussis, *Fluid-Structure Interactions: Slender Structures and Axial Flow*, Vol. 1, Elsevier Academic Press, London, UK, 1998.

[2] M. P. Païdoussis and G. L. Li, "Pipes conveying fluid: a model dynamical problem," *Journal of Fluids and Structures*, vol. 7, no. 2, pp. 137–204, 1993.

[3] J. L. Lopes, M. P. Paidoussis, and C. Semler, "Linear and nonlinear dynamics of cantilevered cylinders in axial flow-part II: the equations of motion," *Journal of Fluids and Structures*, vol. 16, no. 6, pp. 715–737, 2002.

[4] R. A. Ibrahim, "Overview of mechanics of pipes conveying fluids-Part I: fundamental studies," *Journal of Pressure Vessel Technology*, vol. 132, no. 3, pp. 1–32, 2010.

[5] M. Kheiri and M. P. Païdoussis, "On the use of generalized Hamilton's principle for the derivation of the equation of motion of a pipe conveying fluid," *Journal of Fluids and Structures*, vol. 50, pp. 18–24, 2014.

[6] D. B. McIver, "Hamilton's principle for systems of changing mass," *Journal of Engineering Mathematics*, vol. 7, no. 3, pp. 249–261, 1973.

[7] B. Sreejith, K. Jayaraj, N. Ganesan, C. Padmanabhan, P. Chellapandi, and P. Selvaraj, "Finite element analysis of fluid-structure interaction in pipeline systems," *Nuclear Engineering and Design*, vol. 227, no. 3, pp. 313–322, 2004.

[8] L. G. Olson and D. Jamison, "Application of a general purpose finite element method to elastic pipe conveying fluid," *Journal of Fluids and Structures*, vol. 11, no. 2, pp. 207–222, 1997.

[9] U. Lee and H. Oh, "The spectral element model for pipelines conveying internal steady flow," *Engineering Structures*, vol. 25, no. 8, pp. 1045–1055, 2003.

[10] X. Wang and F. Bloom, "Stability issues of concentric pipes conveying steady and pulsatile flows," *Journal of Fluids and Structures*, vol. 15, no. 8, pp. 1137–1152, 2001.

[11] S. Naguleswaran and C. J. H. Williams, "Lateral vibration of pipe conveying fluid," *Journal of Mechanical Engineering Science*, vol. 10, no. 3, pp. 228–238, 1968.

[12] Y. Tang, T. Z. Yang, and B. Fang, "Fractional dynamics of fluid-conveying pipes made of polymer-like materials," *Acta Mechanica Solida Sinica*, vol. 31, no. 2, pp. 243–258, 2018.

[13] I. Mnassri and A. E. Baroudi, "Vibrational frequency analysis of finite elastic tube filled with compressible viscous fluid," *Acta Mechanica Solida Sinica*, vol. 30, no. 4, pp. 435–444, 2017.

[14] X. W. Zhou, H. L. Dai, and L. Wang, "Dynamics of axially functionally graded cantilevered pipes conveying fluid," *Composite Structures*, vol. 190, pp. 112–118, 2018.

[15] W. A. Oke and Y. A. Khulief, "Effect of internal surface damage on vibration behavior of a composite pipe conveying fluid," *Composite Structures*, vol. 194, pp. 104–118, 2018.

[16] B. D. Texier and S. Dorbolo, "Deformations of an elastic pipe submitted to gravity and internal fluid flow," *Journal of Fluids and Structures*, vol. 55, pp. 364–371, 2015.

[17] B. R. Binulal, A. Rajan, and J. Kochupillai, "Dynamic analysis of Coriolis flow meter using Timoshenko beam element," *Flow Measurement and Instrumentation*, vol. 47, pp. 100–109, 2016.

[18] Y. L. Huo and Z. M. Wang, "Dynamic analysis of a vertically deploying/retracting cantilevered pipe conveying fluid," *Journal of Sound and Vibration*, vol. 360, pp. 224–238, 2016.

[19] M. W. Li, Q. Ni, and L. Wang, "Nonlinear dynamics of an underwater slender beam with two axially moving supports," *Ocean Engineering*, vol. 108, pp. 402–415, 2015.

[20] Q. Ni, Y. Y. Luo, M. W. Li, and H. Yan, "Natural frequency and stability analysis of a pipe conveying fluid with axially moving supports immersed in fluid," *Journal of Sound and Vibration*, vol. 403, pp. 173–189, 2017.

[21] F. G. Balmaz, D. Georgievskii, and V. Putkaradze, "Stability of helical tubes conveying fluid," *Journal of Fluids and Structures*, vol. 78, pp. 146–174, 2018.

[22] W. Xia and L. Wang, "Vibration characteristics of fluid-conveying carbon nanotubes with curved longitudinal shape," *Computational Materials Science*, vol. 49, no. 1, pp. 99–103, 2010.

[23] H. M. Ghazavi, H. Molki, and A. A. beigloo, "Nonlinear analysis of the micro/nanotube conveying fluid based on second strain gradient theory," *Applied Mathematical Modelling*, vol. 60, pp. 77–93, 2018.

[24] Y. Guo, J. H. Xie, and L. Wang, "Three-dimensional vibration of cantilevered fluid-conveying micropipes—types of periodic motions and small-scale effect," *International Journal of Non-Linear Mechanics*, vol. 102, pp. 112–135, 2018.

[25] Y. W. Zhang, L. Zhou, B. Fang et al., "Quantum effects on thermal vibration of single-walled carbon nanotubes conveying fluid," *Acta Mechanica Solida Sinica*, vol. 30, no. 5, pp. 550–556, 2017.

[26] L. Wang, Y. Z. Hong, H. L. Dai et al., "Natural frequency and stability tuning of cantilevered CNTs conveying fluid in magnetic field," *Acta Mechanica Solida Sinica*, vol. 29, no. 6, pp. 567–576, 2016.

[27] H. Askari and E. Esmailzadeh, "Forced vibration of fluid conveying carbon nanotubes considering thermal effect and nonlinear foundations," *Composites Part B: Engineering*, vol. 113, no. 15, pp. 31–43, 2017.

[28] H. L. Dai, L. Wang, and Q. Ni, "Dynamics of a fluid-conveying pipe composed of two different materials," *International Journal of Engineering Science*, vol. 73, pp. 67–76, 2013.

[29] J. H. Ginsberg, "The dynamic stability of a pipe conveying pulsatile flow," *International Journal of Engineering Science*, vol. 11, no. 9, pp. 1013–1024, 1973.

[30] M. P. Paidoussis and C. Semler, "Nonlinear and chaotic oscillations of a constrained cantilevered pipe conveying fluid: a full nonlinear analysis," *Nonlinear Dynamics*, vol. 4, no. 6, pp. 655–670, 1993.

[31] L. Wang, Z. Y. Liu, A. Abdelkefi et al., "Nonlinear dynamics of cantilevered pipes conveying fluid: towards a further understanding of the effect of loose constraints," *International Journal of Non-Linear Mechanics*, vol. 95, pp. 19–29, 2017.

[32] W. M. Ji, T. Fang, and S. Q. Chen, *Mechanical Vibration*, Science Press, BeiJing, China, 1985, in Chinese.

[33] B. H. Li, H. S. Gao, Y. S. Liu et al., "Vibration analysis of a multi-span fluid conveying pipe with wave propagation method," *Acta Mechanica Solida Sinica*, vol. 31, no. 1, pp. 67–73, 2010, in Chinese.

[34] B. H. Li, H. S. Gao, H. B Zhai, Y. S. Liu, and Z. F Yue, "Free vibration analysis of multi-span pipe conveying fluid with dynamic stiffness method," *Nuclear Engineering and Design*, vol. 241, no. 3, pp. 666–671, 2011.

[35] S. S. Rao, *Mechanical Vibrations*, Prentice-Hall, Upper Saddle River, NJ, USA, 5th edition, 2011.